AN EXPERIMENTAL INVESTIGATION OF LEADING EDGE SHOCK WAVE-BOUNDARY LAYER INTERACTION AT HYPERSONIC SPEEDS

Thesis by

James M. Kendall, Jr.

In Partial Fulfillment of the Requirements

For the Degree of

Doctor of Philosophy

California Institute of Technology

Pasadena, California

1956

ACKNOWLEDGMENTS

The author wishes to express deep appreciation to Dr. H. T. Nagamatsu and Professor Lester Lees for their encouragement and guidance. He would like to thank the members of the Aeronautics Department machine shop for the construction of various pieces of equipment, Mr. Charles Granneman and Mr. Sam Roman for operation of the wind tunnel, Mrs. Fae Kelley for assistance with the calculations and preparation of the figures, and Mrs. Geraldine Van Gieson for typing the manuscript.

The work discussed in this paper was carried out under the sponsorship and with the financial support of the Office, Chief of Ordnance, and the Office of Ordnance Research, U. S. Army.

ABSTRACT

The boundary layer on a slender body tends to be very thick at hypersonic speeds. It interacts with the external flow by producing larger flow deflections near the leading edge than those due to the body alone. The increased shock strength affects the boundary layer growth. The flow around the boundary layer gives rise to an induced pressure with a negative gradient which thins the boundary layer and increases the skin friction with respect to the zero pressure gradient value.

Experiments on a flat plate with a sharp leading edge ($Re_t < 100$) have been performed in the GALCIT 5 x 5 inch Mach 5.8 hypersonic wind tunnel. The induced pressure was measured by means of orifices in the plate surface. Profiles of Mach number, velocity, mass flow, pressure, and momentum deficiency were calculated from impact pressure surveys normal to the plate surface made at various distances from the leading edge.

The results are as follows: (1) The induced pressures are 25 per cent higher than the weak interaction theory. (2) The boundary layer and the external flow are distinctly separate for Re_x as low as 6000. (3) The shock wave location is in good agreement with that predicted by the Friedrichs theory for a body shape equivalent to the observed boundary layer displacement thickness. (4) Expansion waves reflected from the shock are weak. (5) The average skin friction coefficient tends toward and nearly matches the zero pressure gradient value downstream, but increases to approximately twice that value as the leading edge is approached.

TABLE OF CONTENTS

SYMBOLS

a	speed of sound
C	constant in viscosity relation $\mu/\mu_\infty = C\ T/T_\infty$
C_f	local skin friction coefficient
C_F	average skin friction coefficient
K	similarity parameter $M\theta$
ℓ	Mean free path
M	Mach number
p	static pressure
$\vec{q}$	velocity
Re	Reynolds number per inch
Re_x	Reynolds number based on x
S	entropy
t	leading edge thickness
T	static temperature
u	velocity in x direction
v	velocity in y direction
x	distance from leading edge
y	distance normal to plate surface
γ	ratio of specific heats
δ	boundary layer thickness
δ^*	boundary layer displacement thickness
θ	flow deflection angle
θ'	momentum deficiency $\frac{\rho u}{\rho_\infty u_\infty}\left(1 - \frac{u}{u_\infty}\right) - \frac{1}{\gamma M_\infty^2}\left(\frac{p}{p_\infty} - 1\right)$
μ	viscosity
ν	kinematic viscosity

ρ density

$\bar{\lambda}$ interaction parameter $\dfrac{M^3 \sqrt{C}}{\sqrt{Re_x}}$

$\vec{\omega}$ vorticity $v_x - u_y$

Subscripts

e outside boundary layer edge

s refers to shock wave location

w value at wall

o isentropic stagnation value

∞ undisturbed stream

I. INTRODUCTION

The kinetic energy of a hypersonic flow may be indefinitely larger than its thermal energy. Thus when kinetic energy is converted into heat, small changes in speed such as occur in the inviscid flow field about a slender body are reflected as proportionally large changes in temperature, while at a stagnation point or in an uncooled boundary layer the temperature may rise to many times the free stream value. These large temperature variations serve to distinguish hypersonic flows from supersonic ones with respect to both non-viscous and viscous effects. For example: (1) Small velocity perturbations make such large changes in the local speed of sound that the linearized equations of motion of a supersonic flow are accurate only when the parameter $M\theta$ is everywhere much less than unity. (2) When the Mach number of a flow with fixed static temperature becomes high enough, imperfect gas effects, including dissociation and ionization, will occur because the temperatures become large. (3) The low density of the fluid within the compressible boundary layer enhances the possibility of slip-flow. (4) The thickness of the hypersonic laminar boundary layer tends to increase like M^2 for a given Reynolds number, and may be so great that considerable interaction with the free stream results. This phenomenon is the subject of the present experimental investigation.

So-called shock wave-boundary layer interaction occurs at supersonic speeds when the rapid growth of the boundary layer displacement thickness near the leading edge produces an effective thickening of the body. The resulting disturbance to the oncoming stream adds an induced pressure with a negative gradient to the inviscid pressure. The

induced pressure has a tendency to thin the boundary layer and increase the local skin friction. Simultaneously, the shock wave emanating from the leading edge must increase in strength to account for the added flow deflection, so that streamlines crossing it carry increased values of vorticity and entropy. In this regard, even for bodies which are slender in the usual sense the leading edge thickness is a parameter of great importance because of its strong influence on the shock strength. The streamlines crossing the shock travel very large distances downstream before entering the boundary layer because the relative mass flow in the boundary layer is very small for hypersonic flow. On blunt bodies the pressure induced by interaction is generally insignificant because the boundary layer is kept thin by the high pressures and gradients of the inviscid flow, but on sharp-nosed slender bodies the induced pressure may amount to several times the inviscid pressure.

Several theoretical studies of this problem, principally for a flat plate with an infinitely sharp leading edge, have been made by Bertram[1], Kuo[2], Lees[3, 4], Lees and Probstein[5], Li and Nagamatsu[6], Maslen[7], and Shen[8]. These theories have followed two general approaches. (1) Shen[8] and Li and Nagamatsu[6] have applied the Kármán momentum integral technique to the boundary layer equations in the entire region between the plate surface and the shock wave, not recognizing a boundary layer edge. (2) The other solutions have considered the shock wave and boundary layer as separate, and have calculated the inviscid flow over a body represented by the boundary layer displacement thickness using the concepts of hypersonic similarity and certain approximations. Much of this work is

succinctly reviewed in Refs. 9 and 10. Experiments have been performed by Baldwin[11], Bertram[12], and Hammitt and Bogdonoff[9, 13]. These have been mainly concerned with the measurement of the induced pressure, although an optical determination of the shock wave location has been included in Ref. 13.

It is found that in general the theory does not accurately predict the measured induced pressure distribution. As an extreme example, the induced pressures measured in the helium tunnel [9] are about $2\frac{1}{2}$ times those expected from the theory. Therefore it appears that the theoretical fluid-mechanical model is either deficient in some respect, or is inconsistent with the physical model, especially with regard to the blunt leading edge. These discrepancies have prompted the present experiment. The aim of this experiment has been to measure and map the flow field for the case where the leading edge is so sharp as to be of vanishing importance.

It will be of interest to interpret some of the experimental results in connection with those theories which treat the shock wave and boundary layer as distinct. Therefore some of the concepts involved will be discussed and certain significant parameters deduced by means of order of magnitude estimates.

There exist two regions of flow behind the leading edge shock wave: one near the body surface where viscous or boundary layer

effects predominate because high temperatures cause the viscosity to be large and the density to be small, and an external one where the density is large and the viscosity small, so that dynamic forces predominate. The mass flow deficiency of the hot layer is balanced by an excess mass flow in the cool layer. These regions are distinguished very clearly for the laminar hypersonic boundary layer with no interaction, but near the leading edge where interaction occurs, such a separation of predominating effects is subject to restrictions arising from the boundary layer equations. In Refs. 3 and 6 it has been shown that the Prandtl boundary layer equations remain valid in the presence of interaction as long as $(\delta/x)^2 << 1$. This restriction essentially demands that the pressure variation across the thickness of the boundary layer be small.

Two characteristics of the flow outside the boundary layer are particularly important. (1) The flow is practically inviscid. A comparison of the kinematic viscosity here with that in the boundary layer by means of the linear viscosity relation $\mu/\mu_\infty = C\,T/T_\infty$ gives

$$\frac{\nu_e}{\bar{\nu}} = \frac{1}{C\left(\frac{\bar{T}}{T_e}\right)^2} \sim \frac{1}{C\,M_e^4} << 1$$

where the bars denote average values in the boundary layer. Also, the shear introduced by the curvature of the leading edge shock is much smaller than in the boundary layer. (2) The expansion waves of the flow over the convex boundary layer edge which are incident upon the leading edge shock are practically absorbed there and thus serve to weaken it. For example, according to Ref. 14, the reflected strength

of a wave is less than four per cent at Mach 10 for flow deflections under 40 degrees. It follows from these two characteristics that the flow in this region approximates a simple wave state, so that there exists a relation between the pressure and the flow deflection at every point.

This pressure-angle approximation divides interaction into the categories of weak and strong. For the weak case, the values of $K = M\theta$ are small enough so that the pressure is proportional to θ, corresponding in two dimensions to the first term of the tangent-wedge formula for $K << 1$,

$$\frac{p}{p_\infty} - 1 = \gamma K + \frac{\gamma(1+\gamma)}{4} K^2 + \ldots \qquad \text{(Ref. 10)}$$

The parameter upon which the induced pressure depends may then be deduced. The mass flow in the boundary layer is

$$m = \rho_e \, u_e \, (\delta - \delta^*)$$

and

$$\frac{dm}{dx} = \rho_e \, u_e \left(\frac{d\delta}{dx} - \theta \right) .$$

These give

$$\theta = \frac{d\delta^*}{dx} - \frac{(\delta - \delta^*)}{\rho_e \, u_e} \frac{d(\rho_e \, u_e)}{dx} .$$

On a flat plate, the boundary layer grows like

$$\delta^2 \sim \frac{\bar{\mu} x}{\bar{\rho} \, u_\infty} = \frac{\bar{\mu}/\mu_\infty}{\bar{\rho}/\rho_\infty} \cdot \frac{\mu_\infty \, x}{\rho_\infty \, u_\infty}$$

where $\bar{\mu}/\mu_\infty$ and $\bar{\rho}/\rho_\infty$ take into account the viscous heating. Using the linear viscosity law, and taking $\bar{\rho}/\rho_\infty$ to be $T_\infty/\bar{T}$,

$$\delta \sim \frac{M^2 \sqrt{C}}{\sqrt{Re_x}} \quad x \quad .$$

If θ is taken to be $d\delta^*/dx$, the induced pressure becomes

$$\frac{p}{p_\infty} - 1 = \gamma M \frac{d\delta^*}{dx} \sim \frac{M^3 \sqrt{C}}{\sqrt{Re_x}} \equiv \overline{\chi}$$

In the strong interaction case, K is large and the pressure varies more nearly like θ^2, as in the tangent-wedge formula

$$\frac{p}{p_\infty} - 1 = \frac{\gamma(\gamma+1)}{4} K^2 + \gamma K \left[1 + \left(\frac{\gamma+1}{4}\right)^2 K^2 \right]^{\frac{1}{2}}$$

The same estimate of the boundary layer growth may be made by taking

$$\overline{\rho}/\rho_\infty = T_\infty/\overline{T} \cdot p/p_\infty \quad \text{and} \quad p/p_\infty \sim M^2(\delta/x)^2$$

Then

$$p/p_\infty \sim \frac{M^3 \sqrt{C}}{\sqrt{Re_x}} \quad \text{and} \quad \delta \sim \frac{\sqrt{M}\ C^{1/4}}{Re_x^{1/4}} \quad x$$

The restriction for the Prandtl boundary layer equations to hold becomes

$$\frac{\overline{\chi}}{M^2} << 1 \quad .$$

The occurrence of slip-flow is most probable near the leading edge where the shear is highest, and in the boundary layer where the mean free path, ℓ , is largest. It is assumed that the no-slip condition is satisfied if

$$\ell \frac{du}{dy} << u_\infty$$

This restriction is to be applied to the strong interaction region. In the free stream, $\mu_\infty \sim \rho_\infty \ell_\infty a_\infty$. In the boundary layer $\ell \sim 1/\rho$

so that

$$\frac{\ell}{\ell_\infty} = \frac{T\, p_\infty}{p\, T_\infty} \sim \frac{\sqrt{Re_x}}{M\sqrt{C}} \quad .$$

du/dy is taken to be u_∞/δ, or may be obtained from the theoretical expression for C_f. The restriction becomes

$$\frac{\delta/x}{M} = \frac{1}{\sqrt{M}\ Re_x^{1/4}\ C^{3/4}} << 1 \quad .$$

For a fixed Reynolds number, this is more easily satisfied as the Mach number increases because ℓ decreases faster than the shear increases. In the weak interaction region, the restriction is

$$\frac{\delta/x}{M} = \frac{M}{\sqrt{C}\ \sqrt{Re_x}} << 1 \quad .$$

II. DESCRIPTION OF THE EXPERIMENT

A. Model and Equipment

The experiment was performed in the GALCIT 5 x 5 inch Mach 5.8 hypersonic wind tunnel, which is of the closed-circuit continuously operating type. All tests were made under steady-state conditions. Ahead of the nozzle the air stream was heated to 225°F to prevent air condensation. The supply pressure ranged between 25 and 95 psia, depending on the test-section Reynolds number per inch desired. Extensive facilities are provided for filtering and drying the air. More complete descriptions of the tunnel and its associated instrumentation are to be found in Refs. 15 and 16.

The high carbon steel flat plate model shown in Fig. 1 was seven inches long, five inches wide, and three-eighths inches thick. The bottom of the leading edge was beveled 15°. By comparison with a reference under a high power microscope, the leading edge thickness was estimated to be 0.0002 inches, except at a few places where it was as large as 0.0005 inches. For the measurement of the pressure induced by the growth of the boundary layer, there were 10 orifices in the top surface between x = 0.050 and 4.00 inches spaced approximately equidistantly in the scale $1/\sqrt{x}$. The plate was located in a region of the test-section where the static pressure was constant to within two per cent, and was aligned with the measured flow direction. The flow was regarded as two-dimensional.

Three impact pressure probes with frontal heights 0.0025 (seen in Fig. 1), 0.005, and 0.010 inches were used in surveys of the

flow field about the plate. The tips of the probes were made from stainless steel hypodermic tubing by flattening one end and honing to proper shape. These tips were soldered into off-set holders.

The plate surface pressures were measured by means of a 32-tube vacuum referenced silicone oil manometer. The tubes were read directly to 0.1 mm. The impact pressures were read on a vacuum referenced mercury micromanometer to 0.1 mm.

B. Test Program

The plate surface pressures were measured several times at each of three supply pressures.

Two preliminary tests concerning impact pressure probes were made. First, because a flow deflection of up to 10° behind the leading edge shock was expected, a test of probe sensitivity to angle of attack was made. As the angle of attack of the 0.0025-inch probe was increased from zero, it read 0.1 per cent lower at 3°, 0.5 per cent lower at 6°, and 1.2 per cent lower at 9°. Accordingly, during surveys the probe was maintained at about 4° with respect to the free stream so that the angle of attack error should have been small at every point of measurement. Second, it is well known that when an impact probe being used in boundary layer measurements is large compared to the boundary layer thickness, considerable disturbance to the boundary layer results. Fig. 2 shows the resulting change in the impact pressure profile normal to the plate surface as the size of the probe is increased. The largest of the three probes caused the boundary layer to thicken, and to show a pressure bump at its outer edge characteristic of probe interference. This is

tentatively explained as follows: the static pressure in the vicinity of the probe is increased by the presence of the probe, separating the low dynamic pressure region of the boundary layer for some distance upstream. The resulting deflection of the flow is equivalent to a thickening of the boundary layer, and at the same time increases the efficiency of the shock system in front of the probe, so that it may read higher pressures.

A detailed examination of the flow over the flat plate was undertaken by measuring the impact pressure profiles normal to the plate surface at 10 stations between x = 0.1 and 3.00 inches for each of three supply pressures. The forward limit, x = 0.1 inches, was imposed by the boundary layer being so thin that even the 0.0025-inch probe caused excessive interference.

C. Data Reduction

It was desired to present the induced pressure data as p/p_∞ versus $\overline{\chi}$ in accordance with the interaction theory. p was given by the pressure orifice readings, and p_∞ was taken as the empty-tunnel pressure at the point in space corresponding to each orifice location. The values of M_∞, calculated from the impact pressure ahead of the leading edge shock, were 5.66, 5.79, and 5.80 respectively for the low, medium, and high Reynolds number conditions. The viscosities used in calculating the Reynolds numbers and

$$C = \frac{\mu_w}{\mu_\infty} \frac{T_\infty}{T_w}$$

were determined from the Sutherland formula. For the present case, C = 0.90.

The location of the boundary layer edge, δ, and the shock wave, y_s, were taken from the impact pressure profiles. The artificial definition of δ shown in Fig. 3 is not subject to the usual ambiguity. y_s was taken to be that distance above the plate where the impact pressure reached its maximum value.

Using the impact pressures and an independently determined estimate of either the total pressure (the pressure recovered by an isentropic compression to zero speed) or the static pressure at the same points in space, the following quantities were computed for the intermediate Reynolds number condition: Mach number, velocity, mass flow, momentum deficiency, and either static or total pressure, whichever was not estimated. Isoenergetic flow was assumed.

Outside the boundary layer, the total pressure along a streamline was estimated by determining where that streamline crossed the shock wave by consideration of the mass flow. The measured strength of the shock along its length then determined the total pressure. The details are as follows: (1) The impact pressure ratio across a shock gives an accurate measure of its strength. From the impact pressure profiles a plot of total pressure ratio across the shock as a function of the shock location, y_s, was made. (2) In Fig. 4, several streamlines are shown crossing a curved shock. The y_n's represent the points at which the impact pressure was measured, and the y_{s_n}'s were sought. If $\overline{\rho u}$ is the average mass flow between y_o and y_1, then by continuity,

$$y_{s_1} = y_{s_o} - \frac{\overline{\rho u}}{\rho_\infty u_\infty} (y_o - y_1) \quad .$$

(3) u was taken to be the speed of the flow with negligible error because

the inclination of the flow was small. For a first approximation, $\overline{\rho u}$ was taken equal to the value of ρu at y_o, which was known from the oblique shock relations, and an approximation to y_{s_1} was obtained. (4) The total pressure ratio for this value of y_{s_1} and the impact pressure at y_1 were used to compute ρu at y_1. (5) An improved estimate of $\overline{\rho u}$ was made, and the process repeated until a consistent value of y_{s_1} was obtained. (6) By similar means, y_{s_2} was computed using y_{s_1}, and so on until the streamline being computed crossed the leading edge shock at a value of y_s lower than for which there was information about the shock strength. (7) The other quantities listed above were computed with the aid of the compressible flow tables.

Using the static pressures thus calculated and the measured plate surface pressure, the static pressure was estimated for the remainder of the flow field. The calculations were continued using the impact and static pressures.

θ', the 'momentum' deficiency, has the interpretation of being one-half the contribution of a stream tube to the total drag of a body. θ' is defined by

$$\frac{\rho u}{\rho_\infty u_\infty}\left(1 - u/u_\infty\right) - \frac{1}{\gamma M_\infty^2}\left(\frac{p}{p_\infty} - 1\right) .$$

For the present case, the average drag coefficient at any x-station is given by

$$C_F = \frac{2}{x}\int_0^{y_s} \theta' \, dy$$

Outside the boundary layer, θ' is proportional to the mass flow times the entropy rise through the shock wave, and hence for weak shocks

vanishes like $(M_n^2 - 1)^3$, where M_n is the component of M_∞ normal to the shock.

The mass flow profiles were integrated with respect to y by means of a mechanical integrator, and several streamlines were traced by locating points of equal value of the integral at each x-station. Several Mach lines were traced by a simple quadrature of the sum of the local Mach angle and streamline inclination.

D. Discussion of the Accuracy

The plate surface pressures were measured with less than one per cent error. The scatter of any one orifice reading was occasionally as high as three per cent, but the repeatability of the best straight line in a plot of p/p_∞ versus $1/\sqrt{x}$ was within two per cent. The viscosity used in calculating the Reynolds numbers and C was known to within five per cent, and M_∞ was known to 0.2 per cent, so that $\overline{\chi}$ is accurate to within six per cent.

In the boundary layer, the flow quantity profiles reflect errors due to (1) impact probe location (2) probe error (low Reynolds number effects, etc.) (3) estimated static pressure error (4) assumption of isoenergetic flow. Near the plate surface, errors (2) and (4) are expected to produce large errors in each of the profiles. These errors may, however, be circumvented to some extent by estimating values which are consistent with u/u_∞ being zero at the plate surface and nearly linear in y. At the value of y where $u/u_\infty = 0.5$, u/u_∞, $\rho u/\rho_\infty u_\infty$, M, and p_o/p_{o_∞} may be somewhat affected by errors (2), (3), and (4), but θ', which reaches approximately its maximum there, is relatively unaffected. In the outer boundary layer and in the remainder

of the region where the calculations were based on the estimated static pressure, U/U_∞, $\rho u/\rho_\infty u_\infty$ and M are reasonably accurate, but θ' is not reliable because of its dependence on $(1 - u/u_\infty)$. Since this region extends over at most one-third of y_s, and because θ' is small compared to its maximum, the error contributed to the integral of θ' is small. In the range of y where the calculations were based on the estimated total pressure, all quantities are believed to be nearly as accurate as the measured impact pressures.

One check of the overall accuracy is given by how well the mass flow profiles satisfy the continuity relation

$$\frac{1}{y_s} \int_0^{y_s} \frac{\rho u}{\rho_\infty u_\infty} \, dy = 1 \quad .$$

The value of the integral was 0.97 at x = 0.157 inches, and was between 0.98 and 1.00 for all other stations. It is felt that the integrals of θ' are probably accurate to within five per cent.

III. RESULTS AND DISCUSSION

A. Induced Pressures

The induced pressure ratios are shown versus $1/\sqrt{x}$ in Fig. 5, and versus the interaction parameter $\overline{\chi}$ in Fig. 6. In these figures, the leading edge lies to the right, the trailing edge to the left. Because the Mach number was nearly constant, the present experiment offers no justification for the use of the interaction parameter other than permitting a direct comparison with theory. However, the correlation was improved by including the slight variations of Mach number. Also shown in the latter figure are the first order weak and strong interaction theory results

$$p/p_\infty = 1 + 0.35\,\overline{\chi} \quad \text{and} \quad p/p_\infty = 0.92 + 0.52\,\overline{\chi} \quad \text{(Ref. 10)}.$$

The data are seen to differ from the expected results in two ways: the weak interaction theory should be adequate for $\overline{\chi} < 1$, but the data lie 25 per cent higher; the data are strikingly linear, failing to show any second order variations, or any transition between weak and strong forms.

The discrepancy between the data and the weak interaction theory can be due to: (1) The finite leading edge size in the experiment. This possibility is to be dismissed for two reasons. First, in measuring the induced pressures on a flat plate, Bertram[12] has found that the variation in the plate surface pressure as the leading edge thickness, t, is changed is approximately equal to the corresponding variation of the theoretically calculated pressure of an inviscid flow over a blunt wedge-plate body. In the present experiment, the first pressure

orifice was 250 leading edge thicknesses downstream, and according to Bertram's calculation the leading edge makes a negligible contribution to the measured pressures. Second, no systematic change in the slope of the curves of p/p_∞ versus $\overline{\chi}$ is observed although Re_t has varied by a factor of four.

(2) An inaccuracy of the pressure-angle approximation used in the theory. This will be checked by comparing the tangent-wedge pressure with the measured pressure along a streamline.

(3) An inaccuracy in the theoretical boundary layer growth. This will be checked by comparison with the experimentally determined boundary layer thickness.

(4) Error resulting from the neglect of the second term of the expression

$$\theta = \frac{d\delta^*}{dx} - \frac{(\delta - \delta^*)}{\rho_e u_e} \frac{d(\rho_e u_e)}{dx} .$$

Taking $p/p_\infty = 1 + 0.45 \overline{\chi}$, $\frac{1}{\rho_e u_e} \frac{d(\rho_e u_e)}{dx} = \frac{1}{\gamma p_e} \frac{dp_e}{dx}$,

and $\delta^* = .75\delta \sim \sqrt{x}$, the ratio of the second term to the first becomes

$$r = \frac{0.11 \overline{\chi}}{1 + 0.45 \overline{\chi}} .$$

The flow deflection is underestimated by about seven per cent for $\overline{\chi} = 1$ and by 14 per cent for $\overline{\chi} = 3$.

(5) A pressure variation across the boundary layer thickness. The flow quantity profiles support this possibility.

B. Boundary Layer Growth

The impact pressure surveys were found to define a boundary layer edge very distinctly for even the lowest Re_x, about 6000, where the probe frontal height was 15 per cent of δ. These data are presented in Fig. 7. The straight lines faired through them are proportional to $x^{0.49}$, $x^{0.55}$, and $x^{0.61}$ respectively for the high, medium, and low Reynolds number per inch conditions. In Fig. 8, these data are presented as δ/x versus $\frac{M^2\sqrt{C}}{\sqrt{Re_x}}$ in accordance with theory. The satisfactory correlation is not surprising in view of the good correlation of the induced pressures. The thinning of the boundary layer near the leading edge by the induced pressure is clearly seen, and suggests that δ/x does not exceed some maximum value, in contrast to the infinite value predicted by a simple power law. Thus the requirement $(\delta/x)^2 << 1$ for the Prandtl boundary layer equations to hold may be satisfied.

The boundary layer displacement thickness, δ^*, as defined by

$$\int_0^\delta \rho u \, dy = \rho_e u_e (\delta - \delta^*)$$

may be written

$$\frac{\delta^*}{\delta} = 1 - \frac{1}{\delta} \frac{\rho_\infty u_\infty}{\rho_e u_e} \int_o^\delta \frac{\rho u}{\rho_\infty u_\infty} \, dy \quad .$$

This quantity has been evaluated from the mass flow profiles (which are to be discussed) and is approximately 0.75. According to Fig. 8, the displacement thickness for large Reynolds numbers may then be written

$$\frac{\delta^*}{x} = 0.50 \frac{M^2 \sqrt{C}}{\sqrt{Re_x}} \quad .$$

The value used in the first order weak interaction theory is

$$\frac{\delta^*}{x} = 0.48 \frac{M^2 \sqrt{C}}{\sqrt{Re_x}} \quad .$$

The method of Cohen and Reshotko[17] for calculating the laminar boundary layer with arbitrary pressure gradient was used to predict a boundary layer thickness for the case Re/in. = 117,000. Taking the observed value of δ at x = 0.100 inches as the starting point of the calculation in order to avoid making assumptions about the flow conditions very near the leading edge, and using the measured plate surface pressures, the resulting boundary layer growth was found to agree with the experimental values to within 5 per cent up to x = 3 inches.

C. Shock Wave Location and Strength

The shock location, y_s, is given for three Reynolds numbers in Fig. 7. When these data are presented as Re_y versus Re_x as in Fig. 9, it is found that they may be empirically represented as $Re_y \sim Re_x^{0.90}$. It is interesting to note that in the Princeton helium tunnel at Mach numbers of the order of 14, the shock shape for a flat plate with $Re_t = 119$ may be expressed as $Re_y \sim Re_x^{0.88}$ (Ref. 13).

However, it is perhaps more appropriate to present these data in another way. The shock wave location on a body equivalent to the observed parabolic boundary layer shape

$$\delta^* = 0.50 \frac{M^2 \sqrt{C}}{\sqrt{Re}} \sqrt{x}$$

has been calculated according to the Friedrichs theory, as outlined in Ref. 18, pp. 397-402. In this method, the flow behind the shock is considered to be a simple wave, and the equation of a Mach line may be written

$$y - x \tan\left(\frac{1}{\beta} + \theta\right) = Y(\theta) \quad ,$$

where $\beta = \sqrt{M_\infty^2 - 1}$. Along the shock, dy/dx obtained from this expression must be set equal to $\tan[\eta(\theta)]$, giving the linear differential equation

$$\left\{\tan\left(\frac{1}{\beta} + \theta\right) - \tan\left[\eta(\theta)\right]\right\} \frac{dx}{d\theta} + x \frac{d}{d\theta} \tan\left(\frac{1}{\beta} + \theta\right) = - Y'(\theta) \quad .$$

To the first order one has

$$\tan\left(\frac{1}{\beta} + \theta\right) = \frac{1}{\beta} + 2A\theta$$

$$\tan\left[\eta(\theta)\right] = \frac{1}{\beta} + A\theta$$

where

$$A = \frac{\gamma + 1}{4} \frac{M_\infty^4}{\beta^4} \quad .$$

Integration gives

$$x_s = \frac{1}{A\theta^2} \int_{\theta_o}^{\theta} \theta \, d\, Y(\theta) \quad ,$$

where $\theta_o = \theta$ at $x = 0$. Together with the equation of the Mach lines, this expression gives a parametric representation of the shock shape. Taking $\theta = \frac{d\delta^*}{dx}$, one obtains for the present case

$$Re\left(y_s - \frac{x}{\beta}\right) = 3.13 \, Re_x^{2/3} \quad .$$

This result is shown in Fig. 10, and the experimental data are seen to

compare favorably with the theoretical prediction.

In Fig. 11, the flow deflection behind the shock wave is given for the intermediate value of Re/in. This measure of the shock strength has been determined from the impact pressure ratio across the shock and is considered to be quite accurate. The same quantity has been calculated from the empirical relation $y_s \sim x^{0.88}$, which represents the best fit of the shock location for this value of Re/in. The agreement is seen to be rather poor.

As a check, the reverse procedure was followed. The shock wave angle determined from the impact pressure ratio was integrated by a simple quadrature, starting from the observed shock location at $x = 0.1$ inches. The shock location determined by this means was virtually identical with that measured. It is to be concluded that the determination of the strength of a weak shock by differentiation of its measured location is a matter requiring some care.

D. Flow Quantity Profiles

Certain interesting features of the flow field are disclosed by the profiles of the calculated flow quantities at the various x-stations. One such set of profiles is shown in Fig. 12. For example, the velocity in the viscous region appears to retain the form usual for the laminar compressible boundary layer, while in the external region the velocity is near the free stream value, and the mass flow ratio is larger than unity. The extent to which there exist separate viscous and non-viscous regions does not diminish in the profiles nearer the leading edge. In contrast to the usual viscous flow over a flat plate, the momentum

deficiency does not vanish outside the boundary layer edge, but extends to the shock because of the wave drag of the boundary layer.

A substantial pressure gradient in the y-direction due to the streamline curvature occurs in the inviscid flow region. The mass flow, Mach number, velocity, and momentum deficiency show variations which are consistent. Above a certain value of y, the velocity and Mach number decrease with increasing y because of the increasing static pressure and slowly varying total pressure, while the momentum deficiency increases due to the increasing mass flow. Below this value of y, these quantities show the opposite variation because the total pressure change with y is rapid.

A measure of the vorticity outside the boundary layer edge is afforded by the total pressure profiles. Crocco's theorem is

$$\vec{q} \times \vec{\omega} = - T \nabla S$$

where $\vec{q}$ is the velocity, $\vec{\omega}$ the vorticity $v_x - u_y$, T the temperature, and ∇S the entropy gradient. The entropy may be written

$$S - S_\infty = C_p \ln \left(\frac{p_{o\infty}}{p_o} \right)^{\frac{\gamma-1}{\gamma}} ,$$

and its gradient is approximately

$$\nabla S \doteq \frac{dS}{dy} = \frac{\gamma - 1}{\gamma} C_p \frac{d}{dy} \left(\frac{p_{o\infty} - p_o}{p_o} \right) = R \frac{d}{dy} \left(\frac{\Delta p_o}{p_o} \right) .$$

The vorticity at the plate surface is nearly $\vec{\omega}_w = u_e/\delta$, so that

$$\frac{\vec{\omega}}{\vec{\omega}_w} = \frac{\delta R T}{u_e^2} \frac{d}{dy} \left(\frac{\Delta p_o}{p_o} \right) = \frac{\delta}{\gamma M_e^2} \frac{d}{dy} \left(\frac{\Delta p_o}{p_o} \right) .$$

At x = 0.25 inches, for example $\vec{\omega}/\vec{\omega}_w = 0.1$ outside the boundary layer edge, but is only 0.005 near the shock. The rate of shearing strain $v_x + u_y$ near the shock will be approximately $2u_y < 0$ since $\vec{\omega} \doteq 0$.

Some anomalies remain to be considered. (1) The behaviors of each of the flow quantity profiles near y = 0 reflect the errors suffered by an impact probe at low Reynolds numbers. (2) The profiles at x = 0.157 and 0.250 inches (not shown) show the effects of impact probe interference near $y = \delta$. (3) According to the profiles at x = 0.64 inches and aft, the pressure is about five per cent higher in the boundary layer than in the nearby external region. Although such an effect has not been explained, no reason to discount this result has been found.

E. Flow Field

Fig. 13 gives an experimentally determined representation of the complete flow field. It is seen that the streamlines cross the shock quite far ahead of where they enter the boundary layer, and the Mach lines intersect the shock at very small angles so that the rather slow decay of the shock strength, corresponding to its $x^{0.90}$ shape, is accounted for. The boundary layer growth in the first 0.1 inches determines the shock strength up to about x = 0.7 inches.

In Fig. 14 the static pressure along each of the three most forward Mach lines of Fig. 13 shows only a slight increase with x. Apparently the expansion waves incident upon the shock are reflected as very weak compression waves. The flow deflection along the first Mach line is calculated to be 4.36° at x = 0.157 inches and 4.25° at x = 0.64 inches. This Mach line is nearly straight, having an inclination

15.40° at x = 0.157 inches and 15.21° at x = 0.64 inches. The other Mach lines show smaller variations along their lengths.

The static pressure along the streamline shown crossing the shock at x = 0.1 inches in Fig. 13 has been calculated from the local streamline inclination by means of the tangent-wedge approximation and compared with the pressures taken from the calculated profiles. The results are shown in Fig. 15.

F. Total Drag

Near the leading edge the shear is expected to be higher than the zero pressure gradient value because the boundary layer is thinned by, and $\partial u/\partial y$ at y = 0 increased by, the negative induced pressure gradient. The velocity profiles are not considered to be sufficiently accurate near y = 0 to permit a direct calculation of the local skin friction. Instead, the average skin friction coefficient, C_F, has been obtained from the θ' profiles and is shown in Fig. 16. The drag of the leading edge, approximated as the impact pressure times half the leading edge thickness, is about seven per cent of the measured C_F at x = 0.157 inches, and is less at succeeding stations. Eimer[15] has measured the local skin friction on a flat plate in the same tunnel, and the average skin friction corresponding to his result is shown for comparison. His measurements were made by means of a floating element balance located sufficiently far from the leading edge that interaction effects may be neglected.

Maslen[7] has given a theoretical expression for the local skin friction of the form

$$C_f \sqrt{Re_x} = f(M) + \frac{g(M)}{\sqrt{Re_x}} \quad .$$

It is not directly integrable to give C_F. Instead, the experimental value of C_F at x = 3 inches was taken, and its variation ahead of this station computed from Maslen's result according to the expression

$$C_F = \frac{1}{x} \int_0^x C_f \, dx = \frac{3}{x} C_{F_3} - \frac{1}{x} \int_x^3 C_f \, dx \quad .$$

The values of C_F thus determined agreed with the experimental results to within two per cent.

IV. SUMMARY OF RESULTS

(1) The induced pressures are linear in $\frac{M^3\sqrt{C}}{\sqrt{Re_x}}$ and are about 25 per cent higher than the first order weak interaction theory.

(2) The boundary layer edge is well defined for Re_x at least as small as 6000. The flow outside the edge is inviscid, but vorticity is present.

(3) Away from the leading edge, the boundary layer thickness is in agreement with the zero pressure gradient theory, but is thinner near the leading edge.

(4) The shock wave location may be represented by $Re\,(y_s - \frac{x}{\beta}) \sim Re_x^{2/3}$ and is in good agreement with the theoretical shock location for a parabolic body.

(5) The paths of the Mach lines indicate that the shock location ahead of x = 0.7 inches is determined by the boundary layer growth ahead of x = 0.1 inches. The Mach lines are so nearly parallel to the shock that the strength of the shock along its length decays slowly.

(6) The static pressure and flow deflection are nearly constant along the length of a Mach line, indicating that waves reflected from the shock are weak.

(7) The average skin friction coefficient tends toward and nearly matches the zero pressure gradient value downstream, but increases to approximately twice that value as the leading edge is approached.

REFERENCES

1. Bertram, M. H.: An Approximate Method for Determining the Displacement Effects and Viscous Drag of Laminar Boundary Layers in Two-Dimensional Hypersonic Flow. NACA TN 2773, 1953.

2. Kuo, Y. H.: Viscous Flow Along a Flat Plate Moving at High Supersonic Speeds. J. Aero. Sci., Vol. 23, No. 2, February 1956, pp. 125-136.

3. Lees, L.: On the Boundary Layer Equations in Hypersonic Flow and Their Approximate Solutions. J. Aero. Sci., Vol. 20, No. 2, February, 1953, pp. 143-145.

4. Lees, L.: Influence of the Leading-Edge Shock Wave on the Laminar Boundary Layer at Hypersonic Speeds. GALCIT Technical Report No. 1, July 15, 1954.

5. Lees, L., and Probstein, R. F.: Hypersonic Viscous Flow Over a Flat Plate. Princeton University, Aeronautical Engineering Laboratory Report No. 195, April 20, 1952.

6. Li, Ting-Yi, and Nagamatsu, H.: Shock Wave Effects on the Laminar Skin Friction of an Insulated Flat Plate at Hypersonic Speeds. J. Aero. Sci., Vol. 20, No. 5, May, 1953, pp. 345-355.

7. Maslen, S. H.: Second Approximation to Laminar Compressible Boundary Layer on Flat Plate in Slip-Flow. NACA TN 2818, 1952.

8. Shen, S. F.: An Estimate of Viscosity Effect on the Hypersonic Flow Over an Insulated Wedge. J. Math. and Physics (M. I. T.), Vol. 31, No. 3, October, 1952, pp. 192-205.

9. Hammitt, A. G., and Bogdonoff, S. M.: A Study of Flow About Simple Bodies at Mach Numbers from 11 to 15. WADC Technical Report 54-257, October, 1954.

10. Lees, L.: Hypersonic Flow. Inst. of Aero. Sci., Preprint No. 554, June, 1955.

11. Baldwin, L. C.: Viscous Effects on Static Pressure Distribution for a Slender Cone at a Nominal Mach Number of 5.8. GALCIT Memorandum No. 28, June, 1955.

12. Bertram, M. H.: Viscous and Leading-Edge Thickness Effects on the Pressures on the Surface of a Flat Plate in Hypersonic Flow. J. Aero. Sci., Vol. 21, No. 6, June, 1954, pp. 430-431.

13. Hammitt, A. G., Vas, I. E., and Bogdonoff, S. M.: Leading Edge Effects on the Flow Over a Flat Plate at Hypersonic Speeds. Princeton University, Aeronautical Engineering Laboratory Report No. 326, September, 1955.

14. Eggers, A. J., Jr., and Syvertson, C. A.: Inviscid Flow About Airfoils at High Supersonic Speeds. NACA TN 2646, 1952.

15. Eimer, M., and Nagamatsu, H.: Direct Measurement of Laminar Skin Friction at Hypersonic Speeds. GALCIT Memorandum No. 16, July, 1953.

16. Baloga, P. E., and Nagamatsu, H. T.: Instrumentation of GALCIT Hypersonic Wind Tunnels. GALCIT Memorandum No. 29, July, 1955.

17. Cohen, C. B., and Reshotko, E.: The Compressible Laminar Boundary Layer with Heat Transfer and Arbitrary Pressure Gradient. NACA TN 3326, April, 1955.

18. High Speed Aerodynamics and Jet Propulsion, Vol. VI. Princeton University Press, Princeton, New Jersey, 1954.

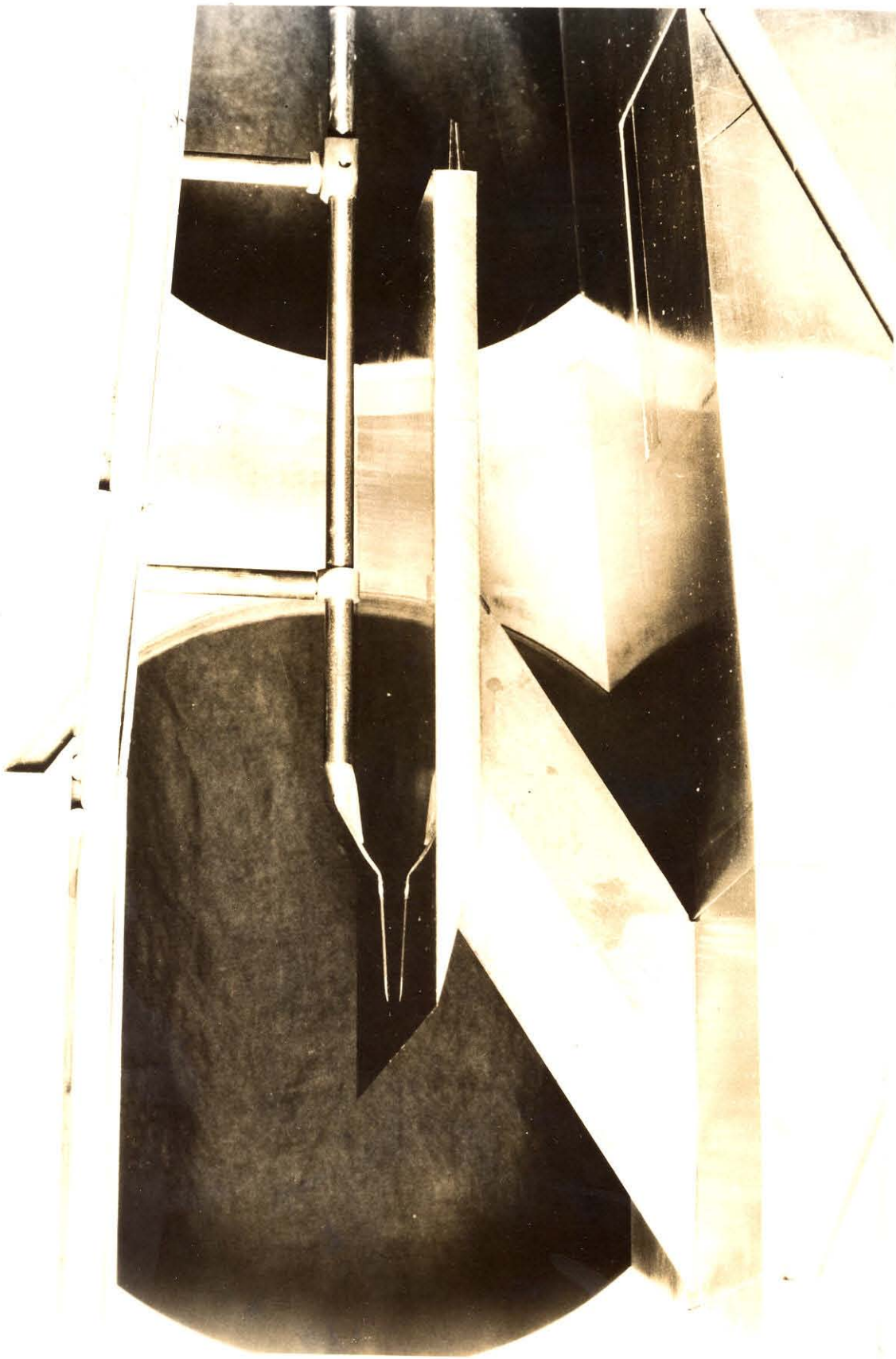

FIG. 1 FLAT PLATE MODEL

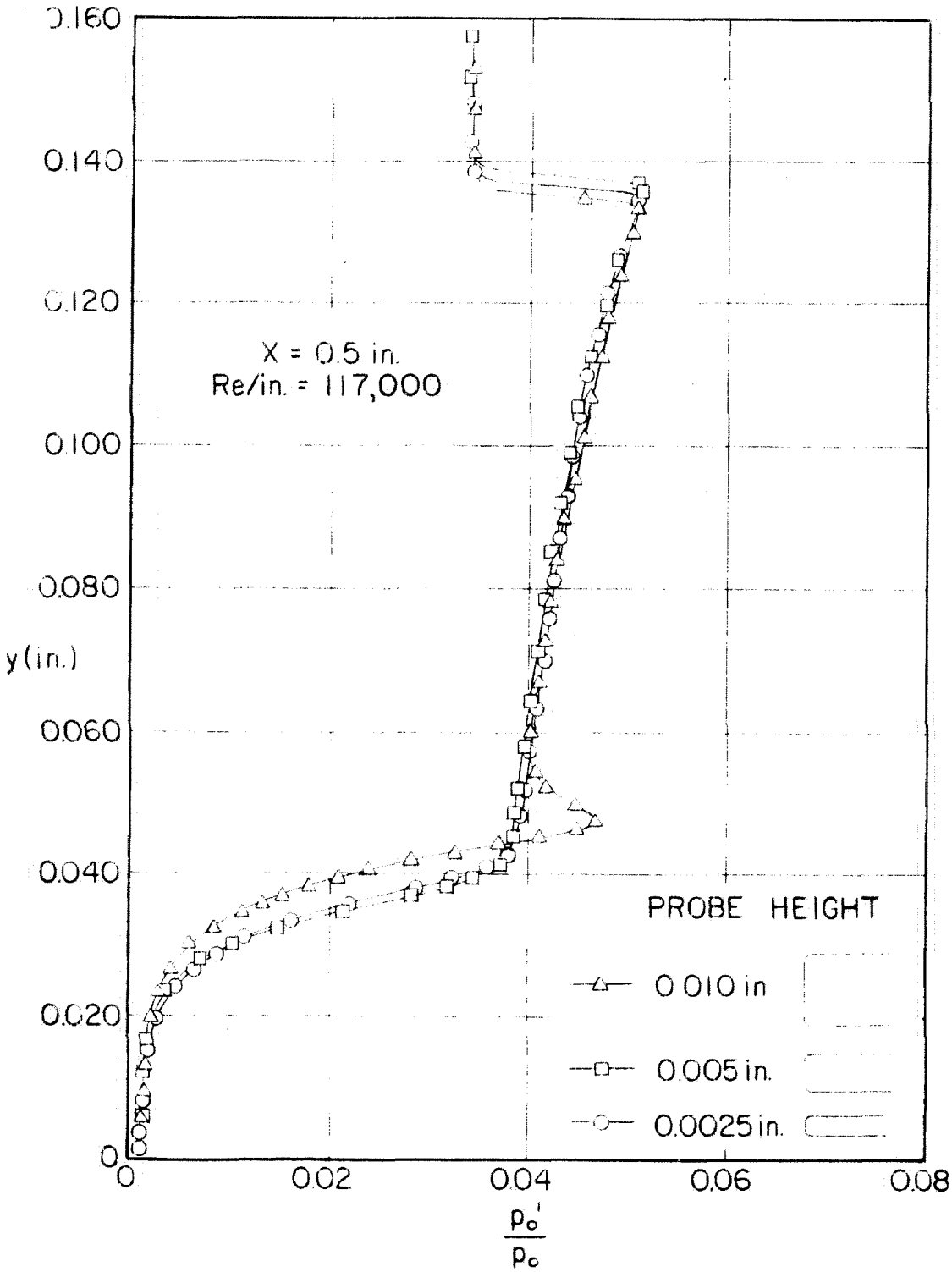

FIG. 2 IMPACT PRESSURE PROFILES

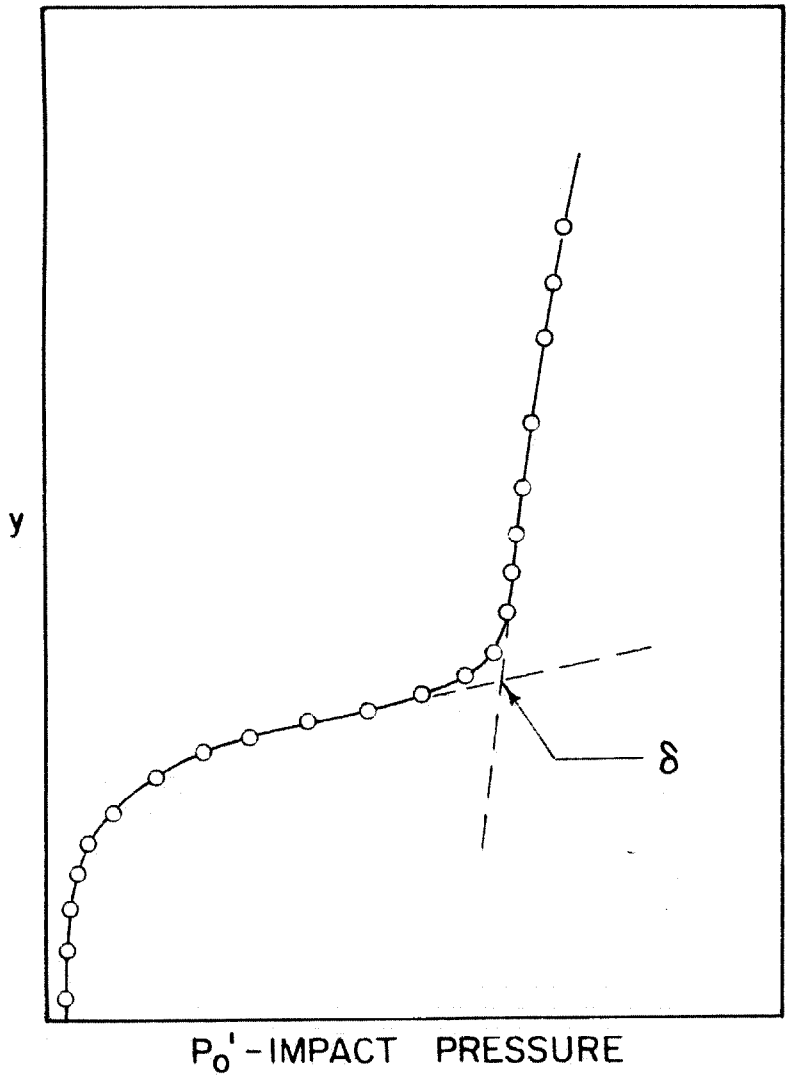

FIG. 3 DEFINITION OF δ

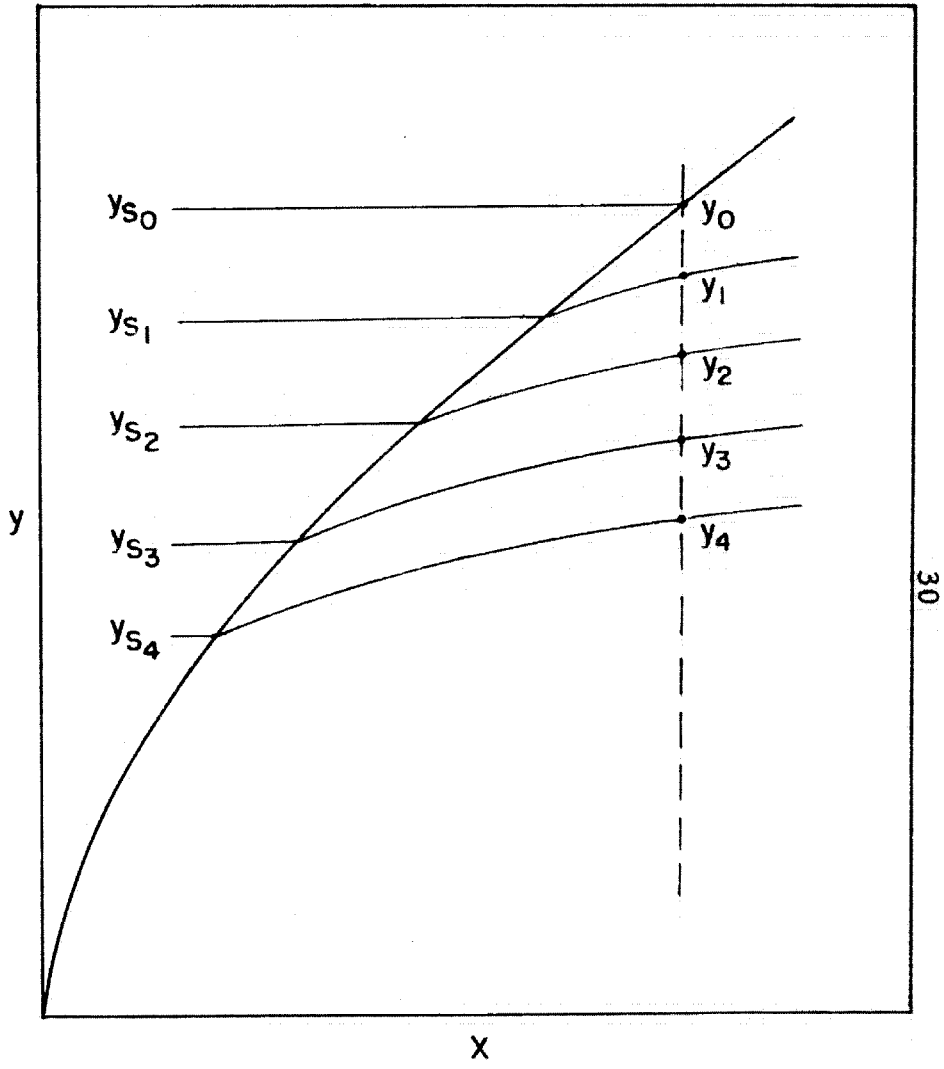

FIG. 4 STREAMLINE PATHS

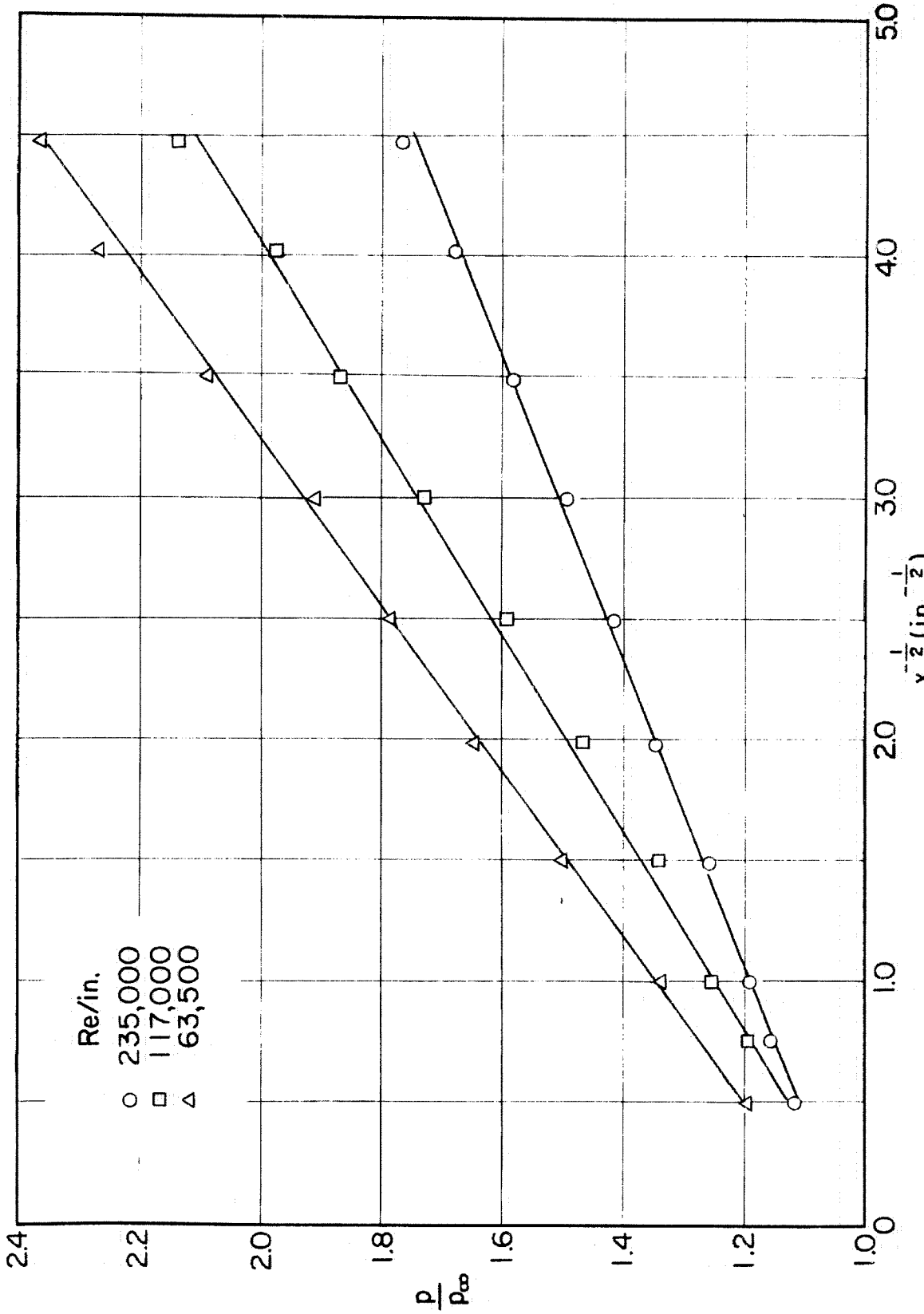

FIG. 5 INDUCED PRESSURE ON A FLAT PLATE AT M=5.8

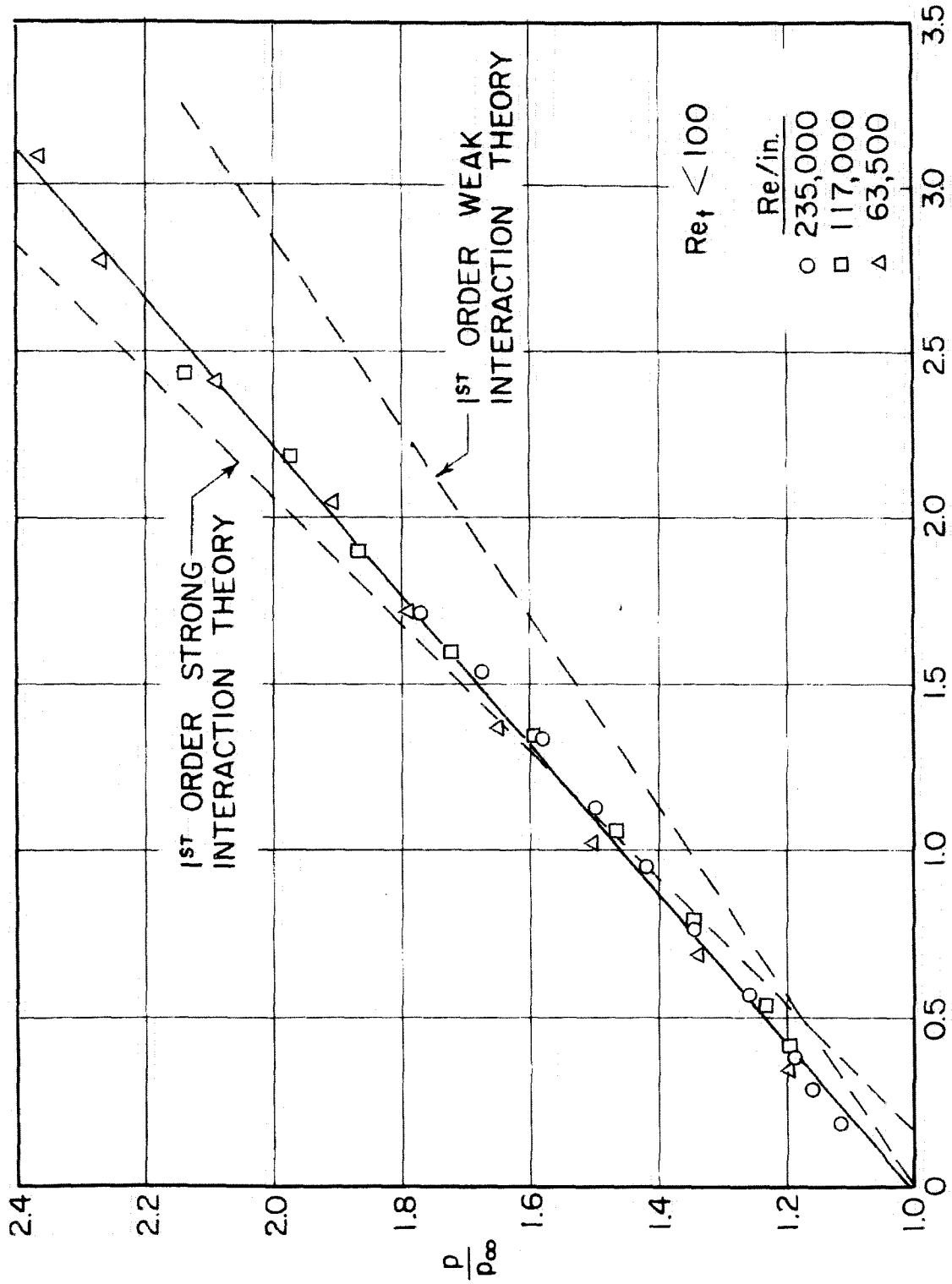

FIG. 6 INDUCED PRESSURE ON A FLAT PLATE AT M = 5.8

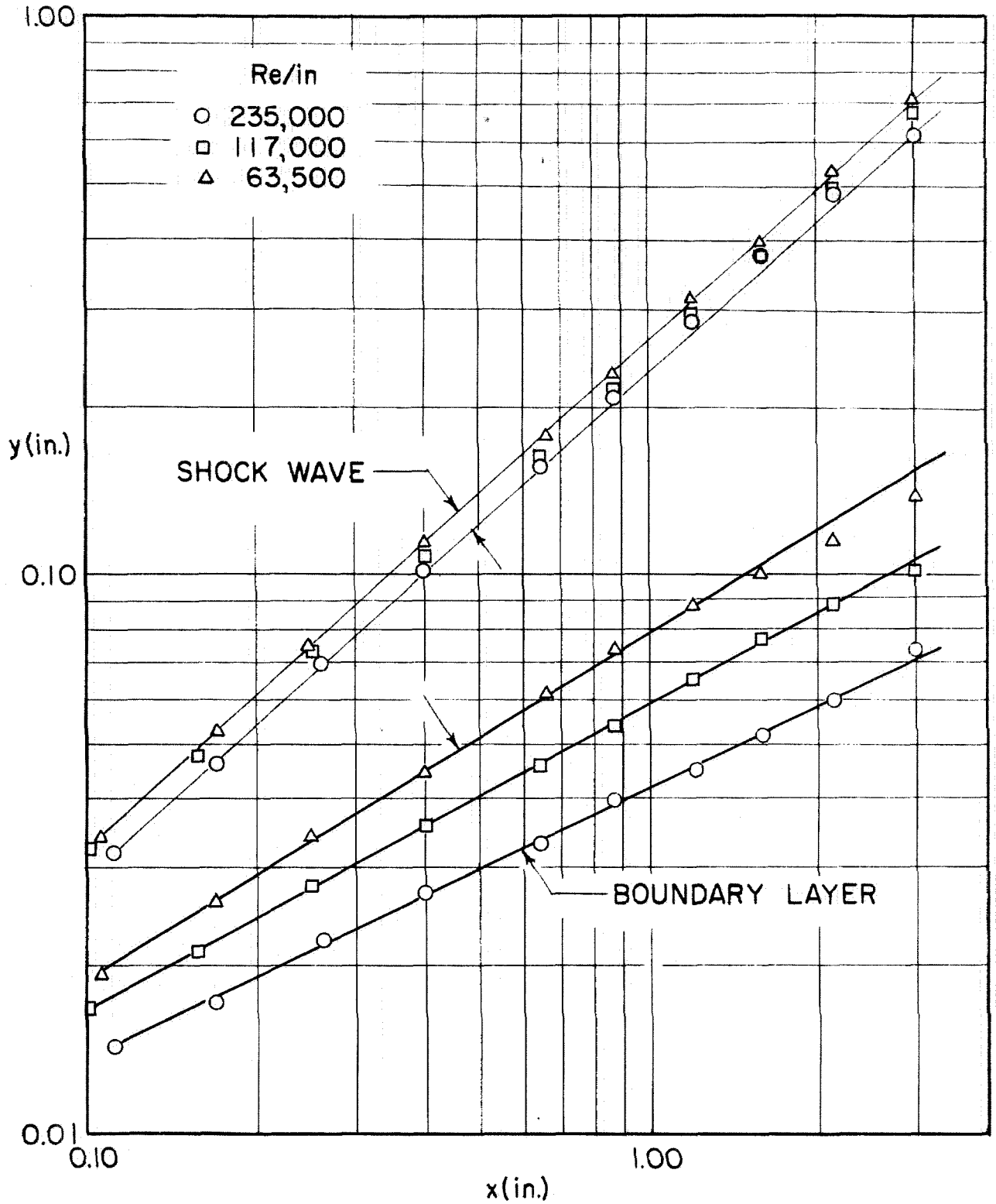

LOCATION OF SHOCK WAVE AND BOUNDARY LAYER EDGE AT M=5.8

FIG. 7

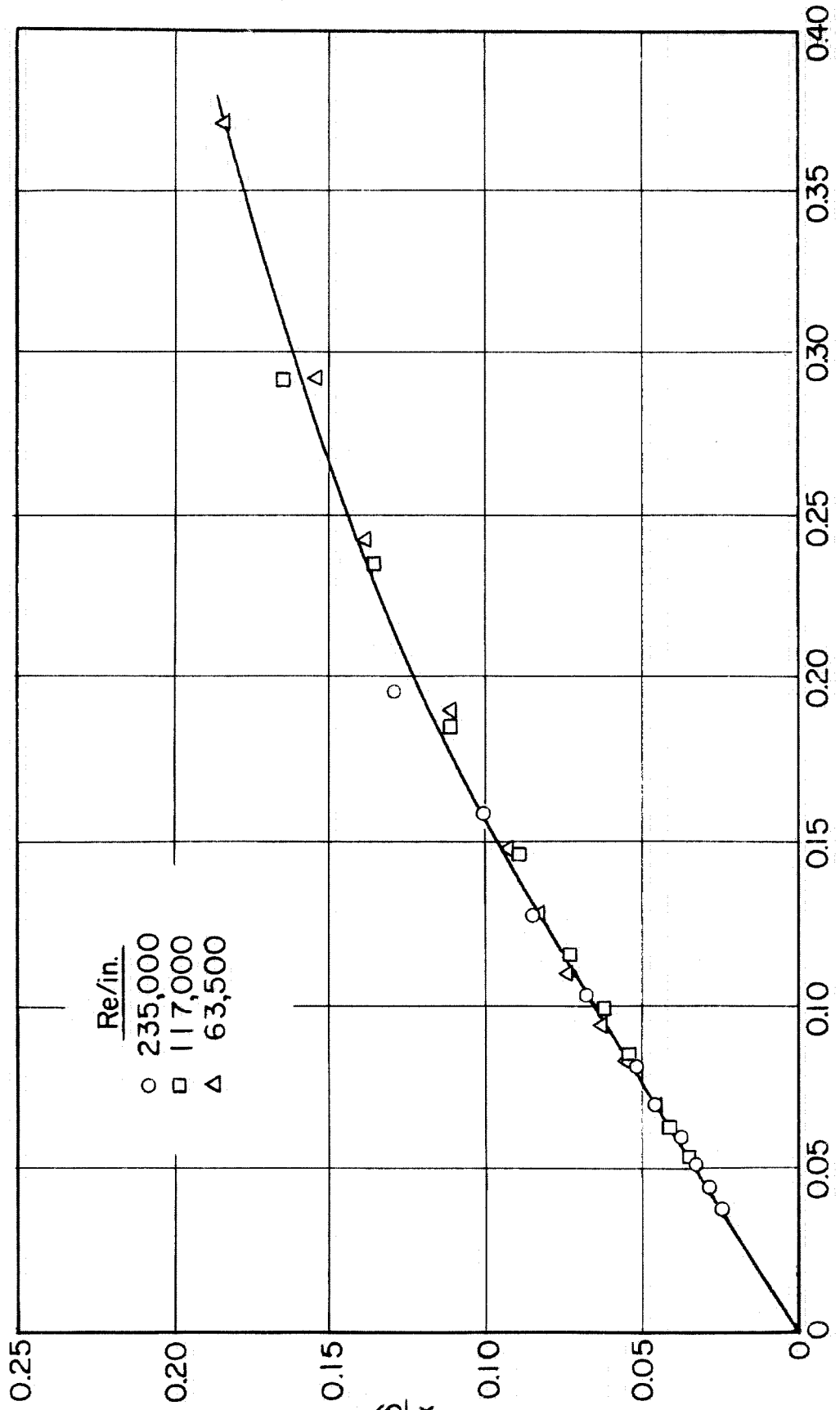

FIG. 8 BOUNDARY LAYER THICKNESS AT M = 5.8

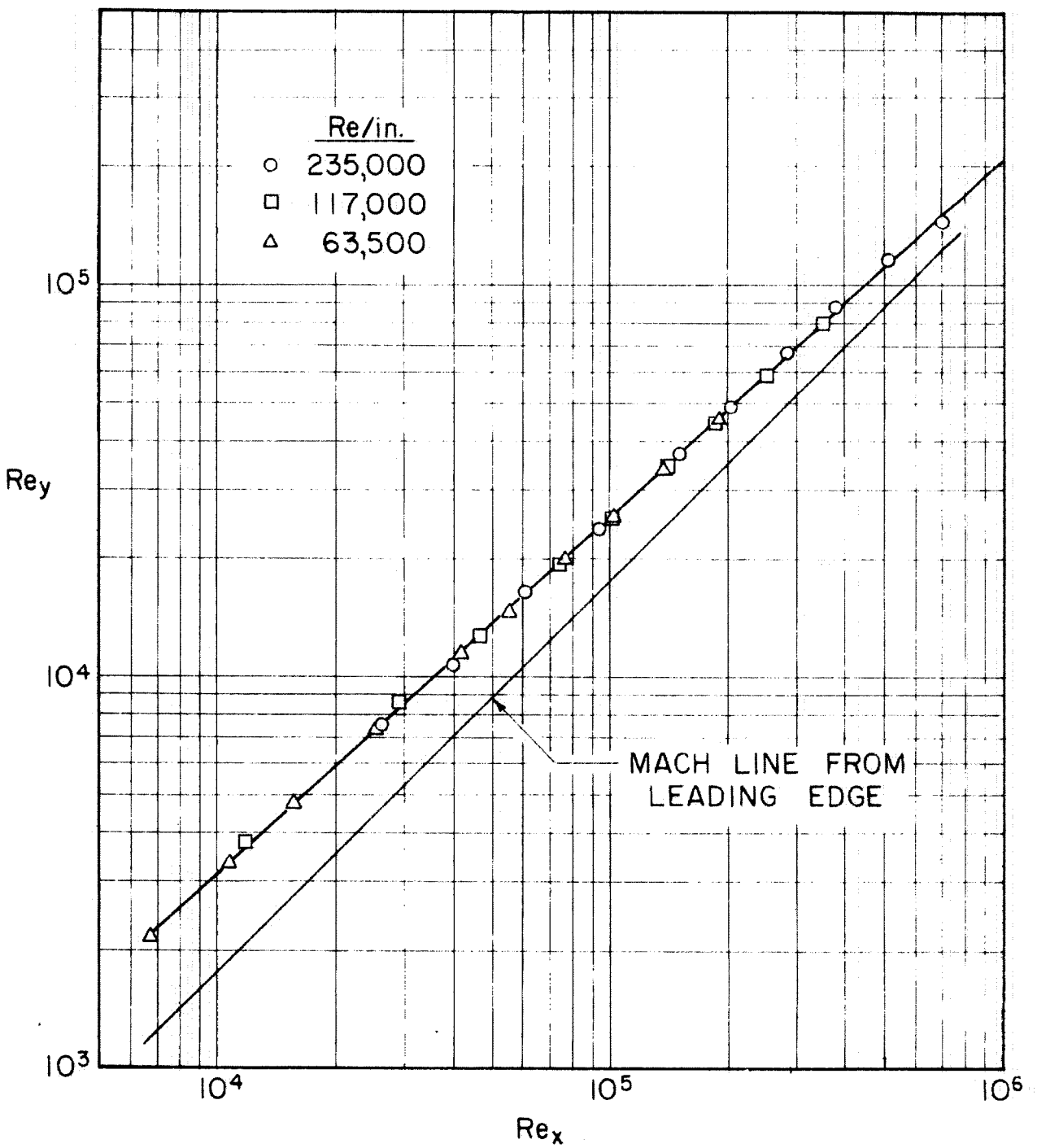

FIG. 9 LOCATION OF SHOCK WAVE

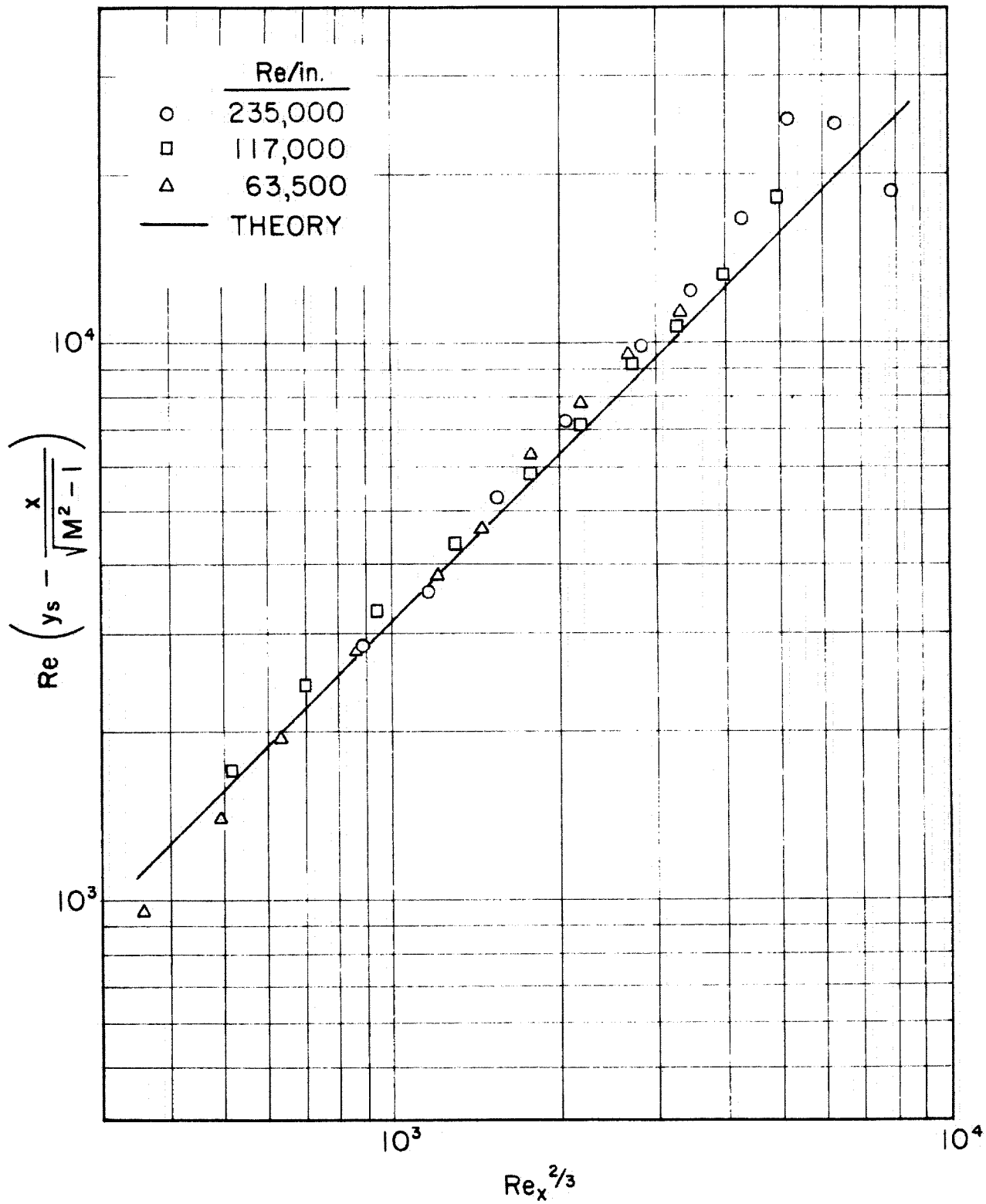

FIG. 10 LOCATION OF SHOCK WAVE

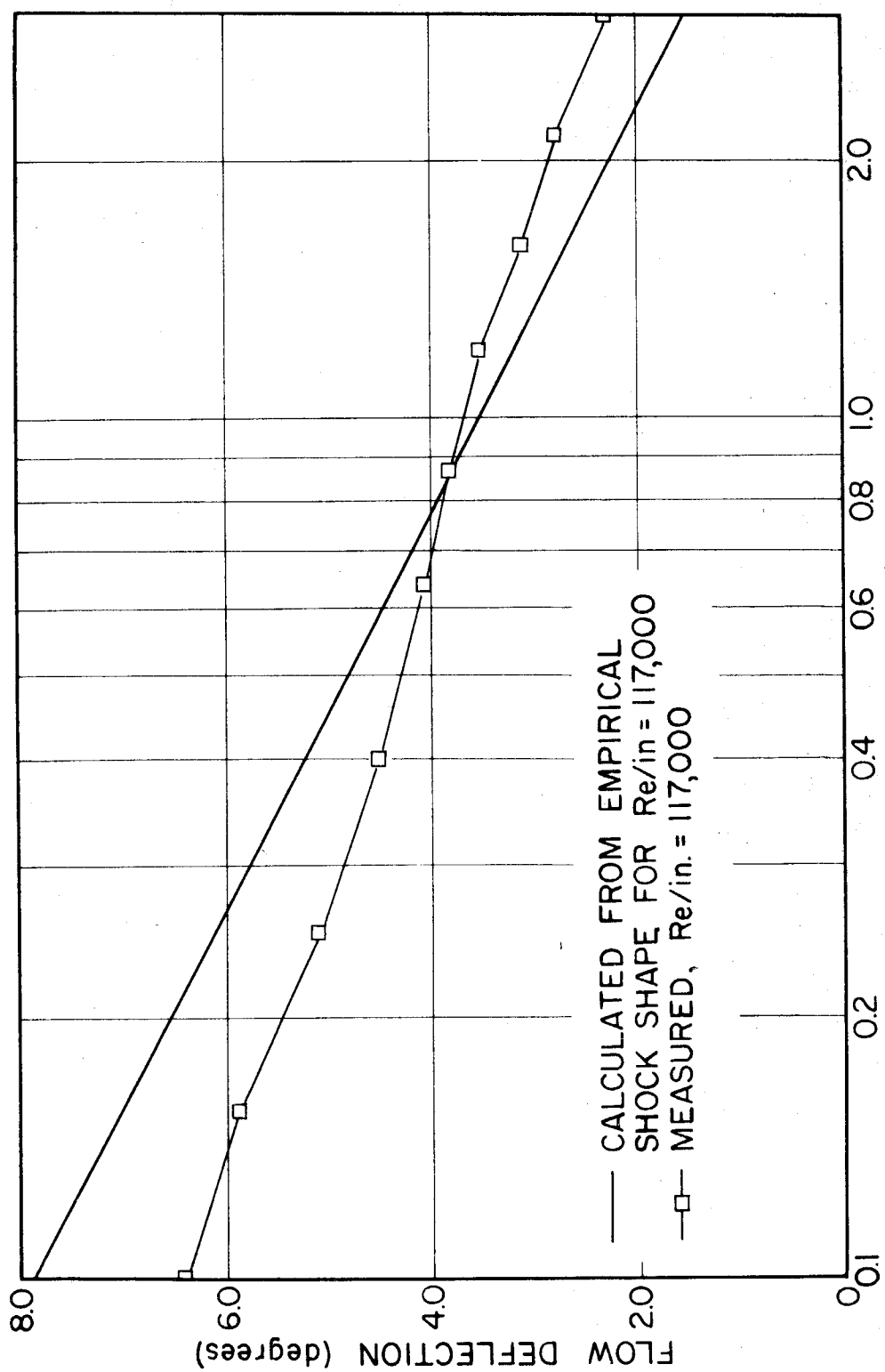

FIG. 11 FLOW DEFLECTION BEHIND LEADING EDGE SHOCK WAVE

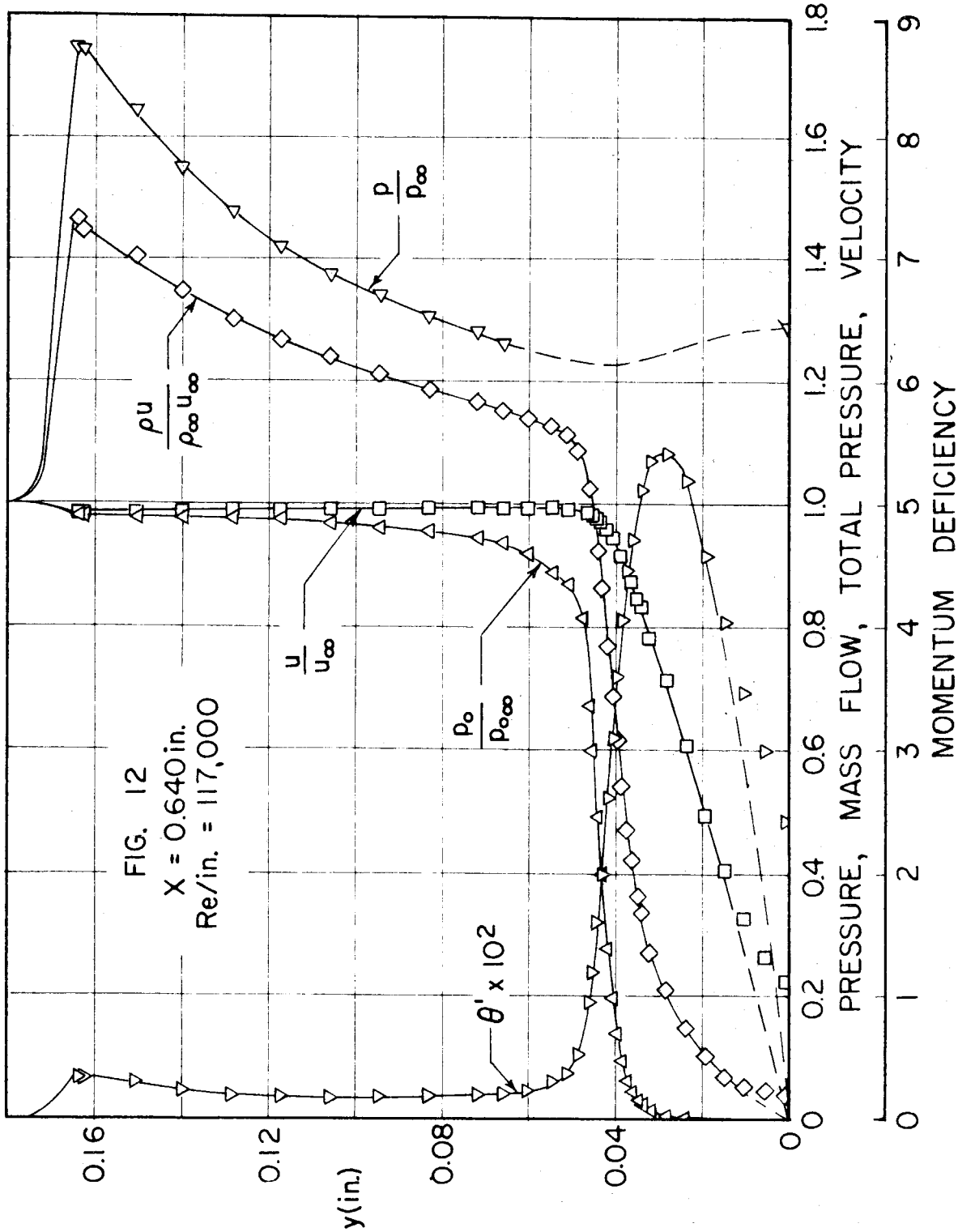
FIG. 12
X = 0.640 in.
Re/in. = 117,000
$\frac{p}{p_\infty}$
$\frac{\rho u}{\rho_\infty u_\infty}$
$\frac{u}{u_\infty}$
$\frac{p_o}{p_{o\infty}}$
$\theta' \times 10^2$
y(in.)
0.16
0.12
0.08
0.04
0
0
0.2
0.4
0.6
0.8
1.0
1.2
1.4
1.6
1.8
1
2
3
4
5
6
7
8
9
PRESSURE, MASS FLOW, TOTAL PRESSURE, VELOCITY
MOMENTUM DEFICIENCY

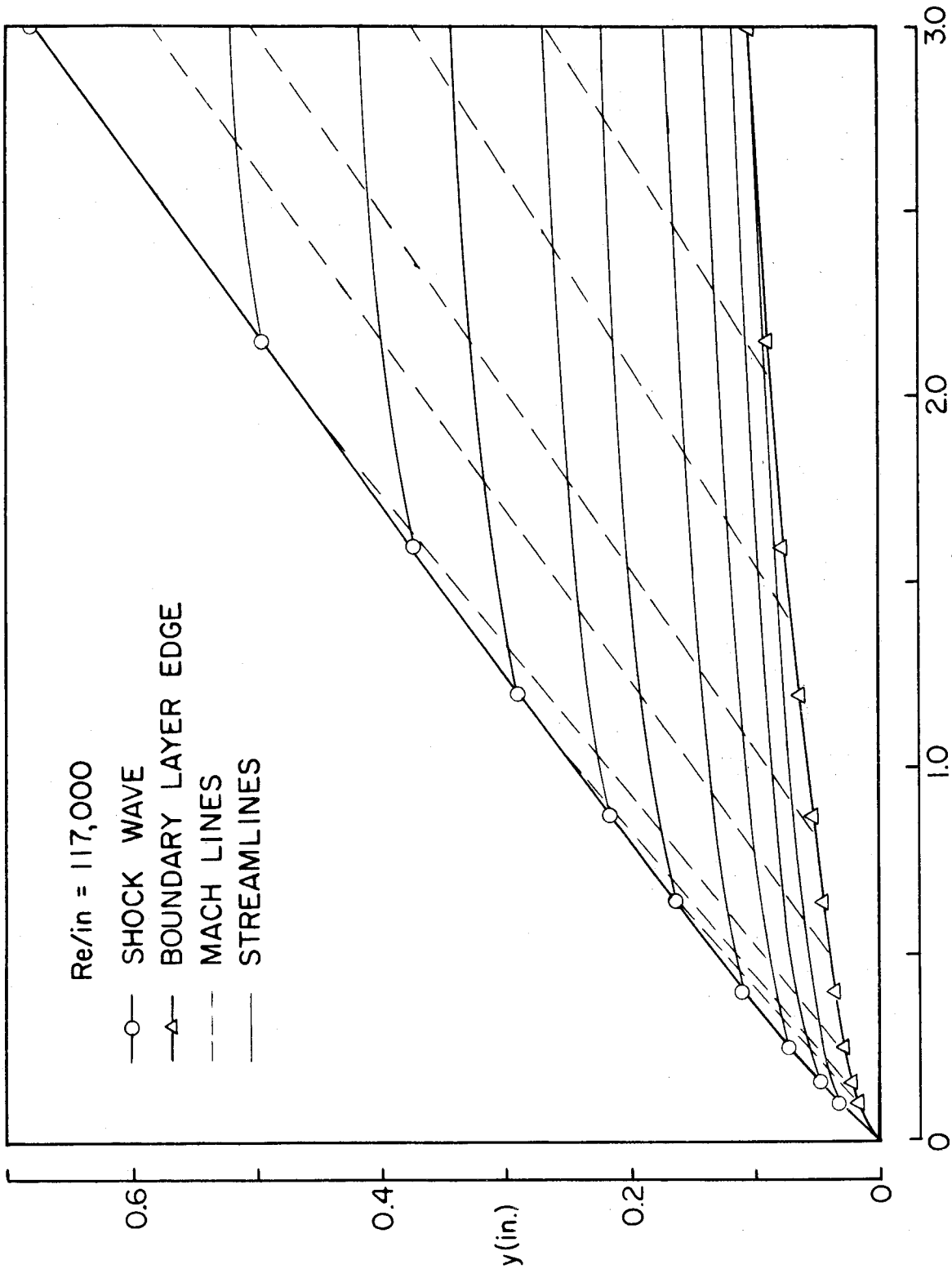

FIG. 13 FLOW OVER A FLAT PLATE AT M=5.8

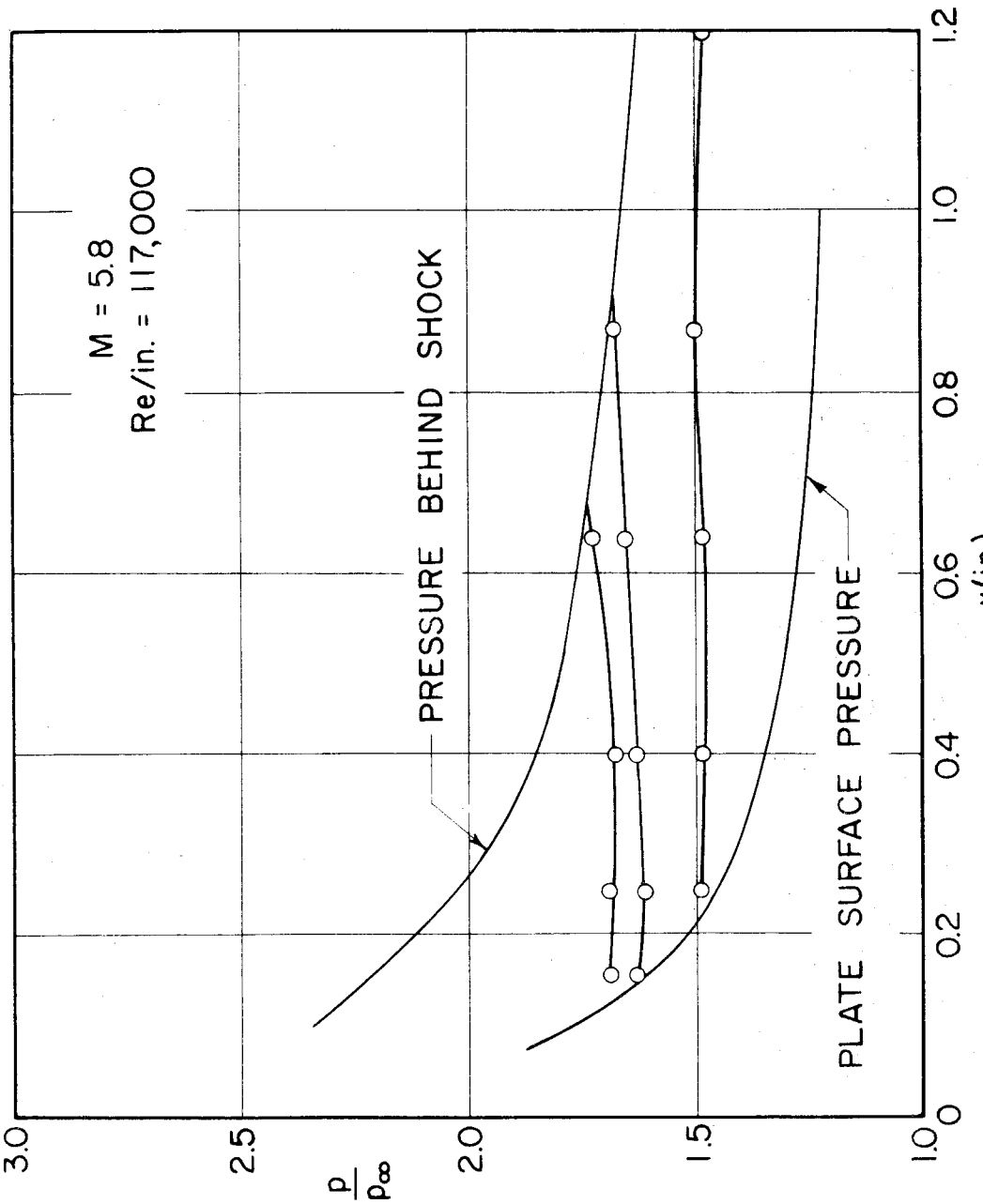

FIG. 14 PRESSURE ALONG MACH LINES

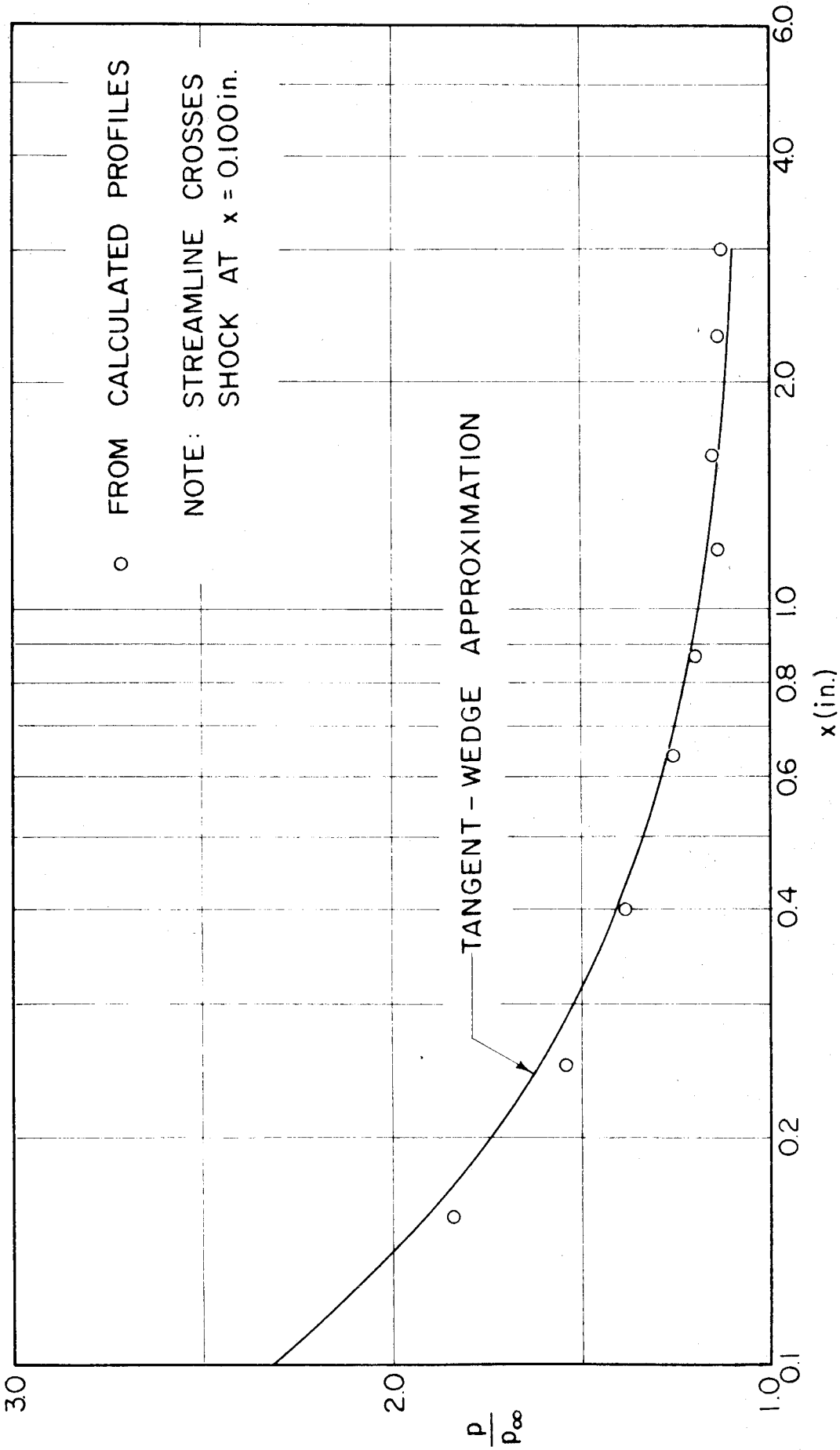

FIG. 15 STATIC PRESSURE ALONG A STREAMLINE

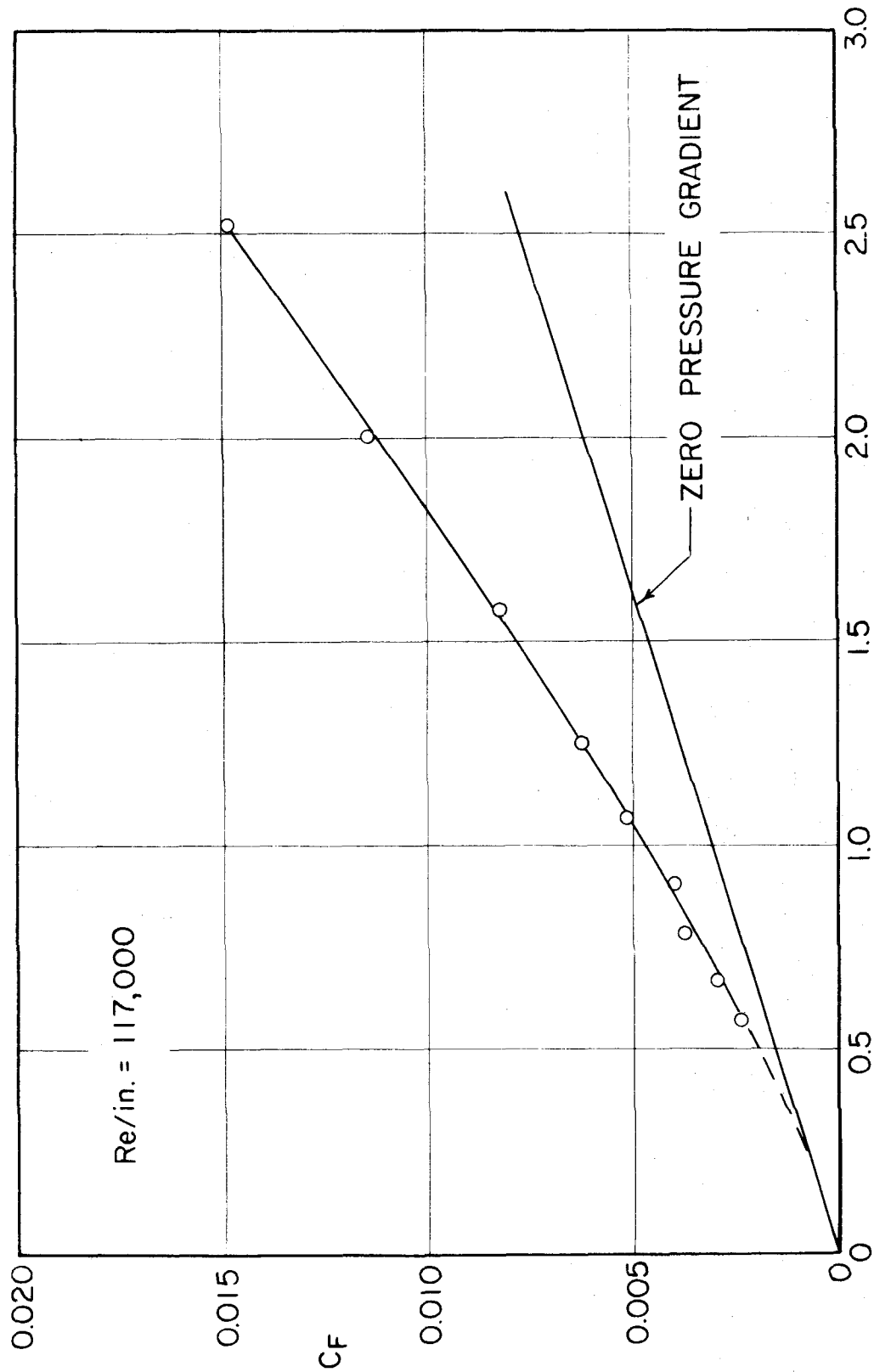

FIG. 16 AVERAGE SKIN FRICTION ON A FLAT PLATE AT M = 5.8